A Method for the Estimation of Defect Detection Probability of Analog/RF Defect-Oriented Tests

John Liaperdos*†, Angela Arapoyanni†, and Yiorgos Tsiatouhas‡
*Technological Educational Institute of Peloponnese, Dept. of Computer Engineering, Sparta 23100, Greece
†National and Kapodistrian University of Athens, Dept. of Informatics and Telecommunications, Athens 15784, Greece
‡University of Ioannina, Dept. of Computer Science & Engineering, Ioannina 45110, Greece

***Abstract*—A method to realistically estimate the defect detection probability achieved by defect-oriented analog/RF integrated circuit tests at the circuit design level is presented in this paper. The proposed method also provides insight to the efficiency of the various available defect-oriented testing techniques, thus allowing the selection of the most suitable for a specific circuit. The effect of structural defects in the presence of process variations and device mismatches is taken into account, by the exploitation of the defect probability distributions and the statistical models of the used technology. Although the proposed methodology is generally applicable to the entire class of analog circuits, its application to simple RF circuits which consist of a few elements seems to be more practical, due to the affordable computational cost implied by circuits with shorter defect dictionaries. In order to obtain results without a reliability compromise, the number of required statistical simulation runs is reduced through regression. The application of the proposed method on a typical RF mixer, designed in a 0.18μm CMOS technology, is also presented.**

I. Introduction

Defect-oriented testing (DOT) [1] of an integrated circuit (IC) focuses on the detection of defects, which correspond to local anomalies that either alter the circuit's topology ('hard' defects, also called structural defects, i.e. shorts, opens, or bridgings), or cause extreme deviation of a circuit's parameter from its nominal value ('soft' defects, also called parametric defects). This particular approach follows the assumption that most or all defect mechanisms manifest themselves in more fundamental observables than the circuit's specifications, thus simplifying the test procedure and also reducing cost.

Defect-oriented testing is a well-established concept in the electronic testing community. The vast majority of DOT techniques, either applied to digital or to analog ICs, are based on the principle of 'defect filters' [2], [3], also referred to as 'signature filters' [4], although often either terms may not be explicitly stated. Derived from a sample of defect-free circuit instances, a defect filter defines an n-dimensional subspace in the space of fundamental observables which compose the circuit's test signature. Circuit instances corresponding to points located inside the subspace defined by the filter are classified as defect-free, while it is assumed that defective instances reside outside the filter's subspace. In the digital domain, for instance, IDDQ may exploit unidimensional or multidimensional 'filters', based on the measurement of a single value of a circuit's quiescence current or on multiple values obtained by the application of different test vectors, respectively [5]. In the analog domain, a unidimensional filter with its fundamental observable corresponding to the time difference of two signals –provided by the test circuitry– has been presented in [6]. Circuit instances may be located on a bidimensional space [7] where an 'acceptance area' –corresponding to a defect filter– is defined in order to discriminate defect-free from defective circuits, while a multidimensional filter –defined by multiple 'variation bands'– may be used for defect-oriented testing [8].

Defect-oriented test generation requires information about all kinds of possible defects, and it is expected to perform better if provided with defect probabilities. This particular information is used to construct a defect list or a defect dictionary, in which all structural defects are included. If the defect dictionary is constructed at circuit level, it is possible for its length to range from hundreds to thousands of defects. In practice, the majority of these defects is unlikely to occur. Inductive fault analysis (IFA) has been proposed [9] to generate realistic defect dictionaries using layout level information. It has also been shown that IFA may significantly reduce the number of defects included in a circuit's defect dictionary [10].

For the case of structural defects, it is reported that spot defects are the dominant cause of yield loss regarding mature processes in high volume production [11]. Although sophisticated models of various physical defects have been proposed for analog/RF circuits, where S-parameters of defects are extracted using an electromagnetic simulator [12], short/bridging and open defects are commonly modeled as fixed resistance values on the order of 1Ω and 10MΩ, respectively [2], [6], [13]–[15]. Recently, the arbitrary selection of fixed resistance values tends to be replaced by their probabilistic distributions [16], [17].

In order to provide an indication regarding the detectability of each defect, variation limits are adopted [7]. Similarly, in [6], defect detection limits are provided for all structural defects included in the defect dictionary under consideration, in order to evaluate the proposed built-in test strategy. However, defects are examined only under typical process conditions. Furthermore, defect detection limits allow the evaluation of a specific DOT technique per defect, while failing to provide a global means of evaluation.

Deterministic fault-coverage, defined as the fraction of detectable defects (in a binary manner) over the total number of defects, is often reported [6], [14], while its probabilistic version, defined as the conditional probability of a device failing the test given that it is indeed defective, seems to provide a more realistic estimation [4], [8], [15]. For the calculation

978-3-9815370-4-8/DATE15/©2015 EDAA

of the latter, relatively large sets of instances are analyzed. A rather arbitrary mixture of subsets of circuit instances subject to common process variations, structural or parametric defects, etc., is selected in [4] in order to form a representative set for test evaluation. The necessity to take common process variations into account while examining structural defects has been recently pointed out. The enhancement of defect simulations with points that represent process spread is recommended in [17], provided that the extra computational effort is affordable. Such an approach is followed in [8]; however, only extreme structural defects are considered.

In this work we present a common method to estimate the detection probability of either a single defect or a complete defect dictionary composed of structural spot defects. The derivation of such a metric takes into account defects in the presence of common process variations and device mismatches. Moreover, defect probability distributions are also considered, while the computational cost associated to circuit statistical simulations is significantly reduced through regression.

The rest of the paper is organized as follows: In Section II, the proposed methodology is formulated, while its application to typical DOT techniques for an RF mixer is presented in Section III. Conclusions are provided in Section IV.

II. Methodology

A. Principle

Let us assume a DOT technique that is based on the measurement of N fundamental observables $O_1, O_2, \ldots, O_N$. In the N-dimensional space of observables we define a variation space ($\mathbf{V}$) to bound defect-free instances of the circuit under test (CUT). A defect filter approach is adopted, according to which a circuit instance is classified as defective if it is located outside the variation space. Note that the construction of the filter is specific to the DOT technique under evaluation, and not an objective of the proposed methodology. All types of structural spot defects included in the circuit's defect dictionary are considered by modification of the CUT netlist, and their characteristic parameters (R) are swept within the range of their limiting values. For each characteristic parameter value a cluster of points in the observable space is obtained by introducing common process variations and device mismatches.

Figure 1, illustrates the case of a three-dimensional space of test observables O_1, O_2, O_3, in which defect-free and defective instance clusters are located. In this figure, a typical short/bridging defect d is considered, whose characteristic parameter corresponds to the resistance value of the short/bridging defect. While this value is swept along its theoretical range (from 0 to ∞), defect clusters ($\mathbf{C}_{R,d}$) tend to converge inside the defect-free variation space. However, this is not always a monotonic behavior, as shown in [7] and as it will be illustrated in the following section.

It is apparent that characteristic parameter values are not equiprobable within their theoretical ranges of variation. Therefore, a realistic evaluation of each defect should also

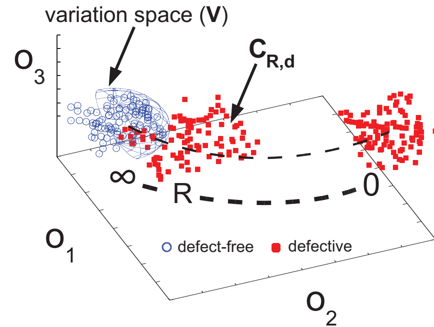

Fig. 1. A three-dimensional space of test observables O_1, O_2, O_3, in which defect-free and defective instance clusters are located. The latter correspond to a specific short/bridging defect d.

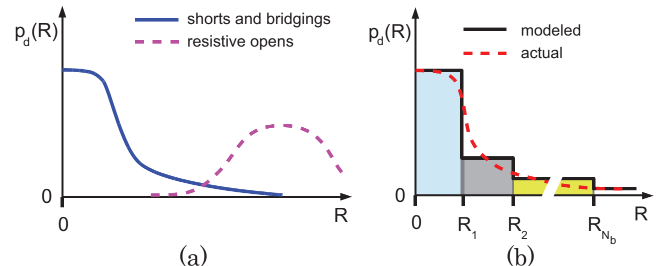

Fig. 2. Probability density function ($p_d(R)$) plots, (a) describing the distribution of characteristic values (R) of common defects, and (b) modeled in piecewise uniform bins (shorts/bridgings case).

take into account the probability distribution of these values. This could be accomplished by considering the probability density functions $p_d(R)$ which describe the distribution of the characteristic parameter R for each defect. Typical probability density function plots, describing the distribution of characteristic values (R) of common defects, are presented in Fig. 2(a).

B. Definitions

In order to make a distinction from deterministic fault coverage, we adopt the term 'defect detection probability' for the probabilistic fault coverage. For a single defect d we define the associated defect detection probability as:

$$P_d = \int_{-\infty}^{\infty} P_{\mathbf{C}_{R,d}}(R) \cdot p_d(R)\,\mathrm{d}R. \qquad (1)$$

$P_{\mathbf{C}_{R,d}}(R)$ represents the corresponding cluster detection probability, defined as:

$$P_{\mathbf{C}_{R,d}}(R) = 1 - \int_{\mathbf{V}} p_{\mathbf{C}_{R,d}}(R)\,\mathrm{d}O_1 \cdots \mathrm{d}O_N, \qquad (2)$$

where $p_{\mathbf{C}_{R,d}}$ is the joint probability density function which describes the distribution of the cluster's points in the N-dimensional space of the $O_1, \ldots, O_N$ observables.

Since cluster points are obtained through statistical simulations, it is more convenient to express the cluster detection probability in discrete form:

$$P_{\mathbf{C}_{R,d}}(R) = \frac{|\mathbf{C}_{R,d} \setminus \mathbf{V}|}{|\mathbf{C}_{R,d}|}, \qquad (3)$$

where $\mathbf{C}_{R,d}$ represents the finite set of points constituting the cluster which corresponds to a characteristic value R for

defect d, and $\mathbf{V}$ represents the infinite set of points inside the variation space.

Characteristic value distributions are identical for specific structural defect classes (i.e. the shorts/bridgings class). Therefore, we can define an overall defect detection probability per class. For a class consisting of N_d defects, the class detection probability is defined as:

$$P_c = \int_{-\infty}^{\infty} P_{\mathbf{C}_R}(R) \cdot p_c(R)\, \mathrm{d}R, \tag{4}$$

where

$$P_{\mathbf{C}_R}(R) = \sum_{d=1}^{N_d} |\mathbf{C}_{R,d} \setminus \mathbf{V}| \cdot \left(\sum_{d=1}^{N_d} |\mathbf{C}_{R,d}| \right)^{-1}. \tag{5}$$

C. Implementation

In a practical situation, it would be impossible to use the integral form of (1) to calculate the detection probability of a defect, due to the continuous nature of its characteristic value R. Nevertheless, measurements on defect monitoring wafers are provided in the form of equiprobable bins [18], as illustrated in Fig. 2(b) which presents the case of the shorts/bridgings class. Assuming N_b bins and $N_{s,i} (i = 1, 2, \ldots, N_b)$ discrete R values within the i-th bin we can obtain the following discrete form for (1):

$$P_d = \sum_{i=1}^{N_b} \sum_{j=1}^{N_{s,i}} \left(\frac{|\mathbf{C}_{R_j,d} \setminus \mathbf{V}|}{|\mathbf{C}_{R_j,d}|} \cdot \frac{P_i}{N_{s,i}} \right), \tag{6}$$

where R_j represents the characteristic value corresponding to the j-th sample in the i-th bin and P_i stands for the probability of the i-th bin, i.e.:

$$P_i = \int_{R_{min,i}}^{R_{max,i}} p_d(R)\, \mathrm{d}R, \tag{7}$$

where $R_{min,i}$, $R_{max,i}$ correspond to the minimum and maximum characteristic parameter values for the i-th bin, respectively.

Similarly, the class detection probability defined in (4) can be computed using the following expression:

$$P_c = \sum_{i=1}^{N_b} \sum_{j=1}^{N_{s,i}} \left(\frac{\sum_{d=1}^{N_d} |\mathbf{C}_{R_j,d} \setminus \mathbf{V}|}{\sum_{d=1}^{N_d} |\mathbf{C}_{R_j,d}|} \cdot \frac{P_i}{N_{s,i}} \right). \tag{8}$$

Finally, a detection probability over all N_c defect classes can be derived:

$$P = \sum_{i=1}^{N_b} \sum_{j=1}^{N_{s,i}} \frac{\sum_{c=1}^{N_c} \left(\sum_{d=1}^{N_{d,c}} \left(\widehat{P}_d \cdot |\mathbf{C}_{R_j,d,c} \setminus \mathbf{V}| \right) \cdot \frac{P_{i,c}}{N_{s,i}} \right)}{\sum_{c=1}^{N_c} \sum_{d=1}^{N_{d,c}} |\mathbf{C}_{R_j,d,c}|}, \tag{9}$$

where $\widehat{P}_d$, which denotes the prior probability of defect d and represents the defect's priority within the defect dictionary, has also been taken into account.

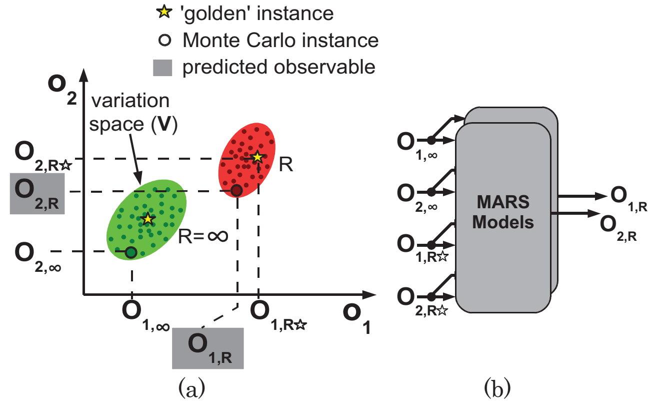

Fig. 3. Cluster points interpolation: (a) Principle, and (b) MARS models used (bidimensional test observable space).

D. Accuracy and computational cost reduction

Equation (6) implies that the most accurate and realistic value for the defect detection probability metric can be obtained only if unlimited computational resources and time are available ($|\mathbf{C}_{R_j,d}| \to \infty$, and $i, j \in [1, \infty)$). However, statistical regression methods, i.e. Multivariate Adaptive Regression Splines (MARS) [19] can be adopted in order to achieve reliable results from a relatively small set of simulation runs.

According to the proposed regression strategy, the characteristic parameter value R can be under-sampled in order to obtain statistical Monte Carlo defect clusters only at specific R values, e.g. at the probability bin boundaries, while the remaining samples are replaced by interpolated cluster points, according to the prediction scheme presented in Fig. 3. Defect cluster instance coordinates $(O_{1,R}, O_{2,R})$ are predicted based on their corresponding counterparts for the defect-free case $(O_{1,\infty}, O_{2,\infty})$ which are input to the MARS models. The latter also require information regarding the coordinates of the 'golden' CUT instance $(O_{1,R\star}, O_{2,R\star})$ within the specific defect cluster. Note that the term 'golden' instance here refers to a CUT fabricated under ideally typical process conditions.

III. Case Study – Simulation Results

The RF Gilbert cell mixer shown in Fig. 4 is used to present the proposed methodology. It is designed in the 0.18μm Mixed-Signal/RF CMOS technology of UMC (Vdd=3.3V). All results were obtained by performing Monte Carlo simulations, taking into account both process variations and device mismatches.

A. Test strategy

1) Test observables: In this case study, we adopt the use of the Local Oscillator's (LO) signal as the test stimulus at the RF inputs of the mixer. Details regarding the test setup and the auxiliary circuitry required are presented in [8]. The self-mixing of the LO signal forces the mixer to operate as a homodyne (zero IF) circuit, generating DC voltage levels at its "IF" outputs. These DC levels (IF_+, IF_-) are used as the test observables, together with the DC voltage component of V_{tail}

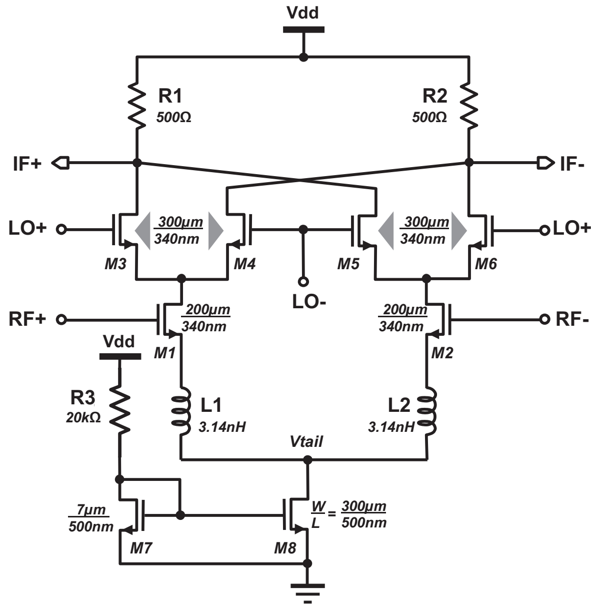

Fig. 4. The RF mixer under consideration.

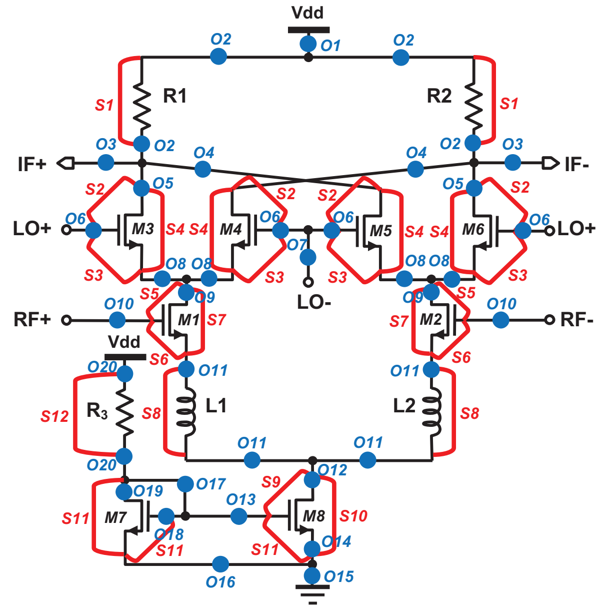

Fig. 5. Injected defects and their codes: (S) Shorts, and (O) Opens.

TABLE I
DEFECT RESISTANCE PROBABILITY DISTRIBUTION

Bin ID	R_{min} (Ω)	R_{max} (Ω)	Bin probability (%)
		Shorts	
1	0	500	69.3
2	500	1k	26.4
3	1k	5k	02.6
		Opens	
1	0	100k	06.0
2	100k	1M	04.0
3	1M	10M	05.0
4	10M	100M	09.0
5	100M	1G	08.0
6	1G	∞	68.0

TABLE II
DEFECT RESISTANCE SAMPLES PER BIN

Bin ID (i)	Resistance samples ($N_{s,i}$)	Resistance sample IDs (cluster ID j)	Resistance sample values (R [in Ω])
		Shorts	
1	4	1–4	0, 125, …, 375
2	5	5–9	500, 600, …, 900
3	11	10–20	1k, 1.4k, …, 5k
		Opens	
1	5	1–5	0, 25k, 50k, 75k, 90k
2	4	6–9	100k, 300k, 600k, 900k
3	3	10–12	1M, 5M, 9M
4	3	13–15	10M, 50M, 90M
5	3	16–18	100M, 500M, 900M
6	2	19–20	1G, 2G

as shown in Fig. 4. In order to demonstrate the application of the proposed technique in two or more dimensions, both a Cartesian plane defined by the (IF_+, IF_-) pair of coordinates and a three-dimensional space defined by (IF_+, IF_-, V_{tail}) are used in our case study as the space of test observables.

2) Variation space: A defect filter approach is adopted, while the variation space is defined as the convex hull of 100 defect-free points in the space of test observables, generated by 100 3σ Monte Carlo simulation runs.

B. Test evaluation

1) Defect dictionary: The examined defect dictionary consists of all possible short and open defects, as shown in Fig. 5. Note that, due to circuit symmetry combined to the symmetrically selected observables, the behavior of some defects is common, therefore they share a common code.

2) Defect probability distributions: Without loss of generality, prior defect probabilities are assumed to be equal. For short and open defects we adopt the resistance distributions shown in Table I [18], [20]. For the case of short defects, only the first three most significant resistance bins are used in calculations, in order to reduce the computational cost.

3) Defect detection metrics: For each individual defect the detection probability, defined by (6), is calculated. The resistance bins and the samples per bin involved in this calculation are presented in Table II, while all defect clusters consist of 100 Monte Carlo 3σ points. Monte Carlo simulations are only conducted for clusters corresponding to resistance sample IDs in $\{1, 5, 10, 20\}$. Simulation data are used for the training of the MARS predictive models which are dedicated to the interpolation of the remaining cluster points. Since the defects under consideration belong to the short/open defect classes, (8) is used to calculate the overall detection probability for each class, while the total defect detection probability over both classes is derived using (9). Fault coverage and detection limits are also reported for the sake of comparison.

C. Results

1) Case-1: Bidimensional test observable space: The various defect detection metrics obtained from the application of the proposed methodology relying on the pair (IF_+, IF_-) of observables are presented in Table III, in which resistance detection limits are calculated as the maximum (minimum) resistance values for which a short (open) defect

TABLE III
DEFECT DETECTION METRICS OBTAINED USING (IF_+, IF_-) AND (IF_+, IF_-, V_{tail})

Defect Code	(IF_+, IF_-)				(IF_+, IF_-, V_{tail})			
	Defect coverage (%)	Upper/Lower Detectable Resistance Limit (Ω)	Defect Detection Probability (%)		Defect coverage (%)	Upper/Lower Detectable Resistance Limit (Ω)	Defect Detection Probability (%)	
			Actual cluster points	Predicted cluster points			Actual cluster points	Predicted cluster points
S1	100	>5k	98.02	97.88	100	>5k	98.10	98.02
S2	0	*undetectable*	31.07	32.97	0	*undetectable*	42.23	44.94
S3	100	3.8k	97.56	97.59	100	3.8k	97.77	97.81
S4	100	2.6k	97.18	97.18	100	2.6k	97.40	97.40
S5	100	250	47.95	47.79	100	375	61.01	58.99
S6	100	125	65.13	67.56	100	>5k	94.45	94.45
S7	100	500	68.83	65.99	100	600	84.59	83.81
S8	100	125	20.66	21.68	100	125	31.66	33.33
S9	100	>5k	98.30	98.30	100	>5k	98.30	98.30
S10	100	375	61.05	60.78	100	375	72.56	69.72
S11	100	>5k	98.30	98.30	100	>5k	98.30	98.30
S12	100	>5k	98.30	98.30	100	>5k	98.30	98.30
ALL	*85.71*	–	*73.53*	*73.74*	*85.71*	–	*80.47*	*80.68*
O1	100	25k	98.86	98.86	100	25k	99.02	99.02
O2	100	25k	98.91	98.91	100	25k	99.04	99.04
O3	100	25k	98.84	98.84	100	25k	98.98	98.98
O4	100	25k	98.84	98.84	100	25k	98.98	98.98
O5	100	25k	98.84	98.84	100	25k	98.97	98.97
O6	100	25k	98.91	98.91	100	25k	99.04	99.04
O7	0	*undetectable*	24.52	23.12	0	*undetectable*	36.41	34.65
O8	100	25k	98.84	98.84	100	25k	98.98	98.98
O9	100	25k	98.84	98.84	100	25k	98.98	98.98
O10	100	25k	98.84	98.84	100	25k	98.98	98.98
O11	100	25k	61.49	61.99	100	25k	98.96	98.96
O12	100	25k	98.85	98.85	100	25k	98.97	98.97
O13	0	*undetectable*	11.69	11.12	0	*undetectable*	22.87	23.43
O14	100	25k	98.87	98.87	100	25k	99.02	99.02
O15	100	25k	98.86	98.86	100	25k	98.99	98.99
O16	100	25k	98.86	98.86	100	25k	99.02	99.02
O17	0	*undetectable*	11.31	10.91	0	*undetectable*	22.71	23.57
O18	0	*undetectable*	05.81	05.70	0	*undetectable*	19.63	19.02
O19	100	25k	98.88	98.88	100	25k	99.02	99.02
O20	100	25k	98.87	98.87	100	25k	98.99	98.99
ALL	*87.18*	–	*84.35*	*84.30*	*87.18*	–	*89.84*	*89.77*
TOTAL	*86.45*	–	*78.91*	*79.02*	*86.45*	–	*85.16*	*85.23*

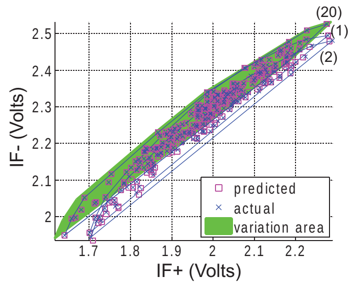

Fig. 6. Points of selected clusters for the S2 defect (bidimensional case, cluster IDs in brackets).

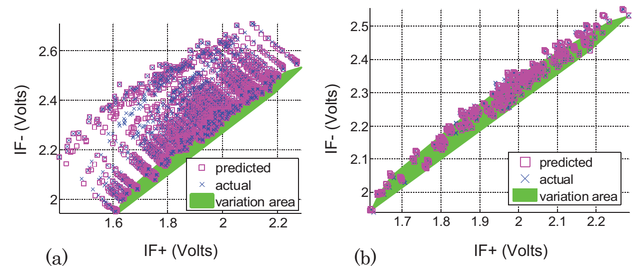

Fig. 7. Cluster points for (a) the S4 defect and (b) the O7 defect (bidimensional case).

in the pertinent 'golden' instance remains detectable. It can be observed that defect coverage might be misleading due to its binary definition. The S2 defect, for instance, is classified as undetectable since all 'golden' cluster instances fall inside the variation area. However, this defect seems to be partially detectable in fact, since 31.07% of all cluster points are located outside the defect filter boundary, as concluded from Table III and graphically represented in Fig. 6. Similar conclusions can be derived for the O7 defect, whose cluster points are shown in Fig. 7(b). On the other hand, the S1 defect would be classified as fully detectable, considering either defect coverage or upper detectable resistance limit. Nevertheless, this seems not to be absolutely true, since a small amount of defective instances (about 2%) remain undetectable. These observations explain the significant discrepancies between defect coverage and defect detection probability.

From the examination of the metrics presented in Table III, it can further be concluded that detection probabilities calculated from the predicted defect clusters adequately match their counterparts derived by actual simulations. Even in the cases where interpolation accuracy is degraded, detection probability calculations remain highly accurate. This is due to the fact that degraded interpolation accuracy is compensated from the large distance between the corresponding clusters and the variation area. For instance, this observation is illustrated in the S4 defect case shown in Fig. 7(a) where larger prediction errors occur for points that are distant from the variation area, while prediction accuracy increases as points tend to converge to the defect-free cluster.

The examination of the S2 defect, whose behavior is pre-

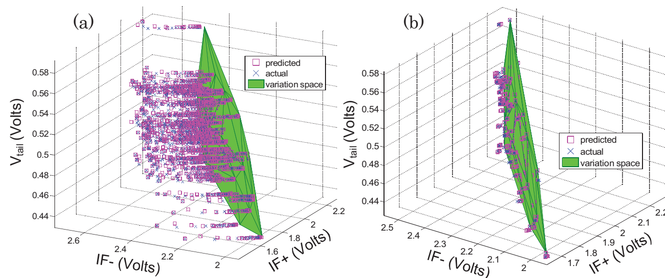

Fig. 8. Cluster points for (a) the S4 defect and (b) the O7 defect (three-dimensional case).

sented in Fig. 6, leads to some further interesting remarks. This is a non-monotonic defect, since its defect clusters might either approach or recede the variation area while resistance is swept from 0 to ∞. As it can be observed, cluster-1 is located closer to the defect-free area compared to cluster-2, although the defect resistance is lower in the first case. Furthermore, due to the proximity of the defect clusters, a high interpolation accuracy is maintained, which leads to an analogously high correlation between actual detection probability calculations and their predicted counterparts, as shown in Table III.

2) Case-2: Three-dimensional test observable space: The test relying on (IF_+, IF_-, V_{tail}) has also been considered, and the corresponding defect detection metrics are presented in Table III, while Fig. 8 corresponds to the three-dimensional version of Fig. 7. Results confirm that defect coverage fails to adequately match defect detection probability, especially in the shorts case. More specifically, although the detection of shorts is significantly improved with the introduction of V_{tail} as an additional observable, defect coverage maintains the same value as when V_{tail} is ignored, as concluded from the comparison of the results which correspond to the two cases presented in Table III.

D. Discussion

A major concern regarding the proposed method is the computational cost implied by the conduction of statistical simulations. A duration of 3 minutes per a 100-point cluster is reported for the simulation time related to our case study, exploiting the computational resources provided by a personal computer equipped with a 4-core 2.2GHz processor. For the specific defect dictionary, 32 hours of simulation would be required to obtain data for the 20 discrete resistance values being swept. This is 5 times the duration that would be necessary if MARS interpolation was used. Note that a further computational cost reduction is expected if layout information is available. This would allow the elimination of some possible defects, making the defect dictionary smaller.

IV. Conclusions

In this paper, a method to estimate the defect detection probability achieved by defect-oriented analog/RF integrated circuit tests at the circuit design level was presented. This method abandons the approach of defects being injected in a circuit's instance corresponding to typical process conditions and also takes into account the effect of process variations and device mismatches. Defect detection probability can be calculated in a defect, a defect class, or an entire defect dictionary basis, also allowing comparison of various DOT techniques. The computation effort required for the derivation of the proposed defect detection capability was adequately kept within practical limits by reducing the number of simulation runs through regression. The extension of the proposed method for the determination of other useful test metrics, such as yield loss and test escape, remains a subject for future work.

References

[1] M. Sachdev and J. P. de Gyvez, *Defect-Oriented Testing for Nano-Metric CMOS VLSI Circuits*. New York: Springer, 2007.

[2] H. G. Stratigopoulos, S. Mir, E. Acar, and S. Ozev, "Defect filter for alternate RF test," in *Proc. IEEE European Test Symp.*, 2009, pp. 161–166.

[3] N. Kupp, P. Drineas, M. Slamani, and Y. Makris, "Confidence estimation in non-RF to RF correlation-based specification test compaction," in *Proc. 13th European Test Symp. (ETS)*, 2008, pp. 35–40.

[4] S. S. Akbay and A. Chatterjee, "Fault-based alternate test of RF components," in *Proc. IEEE Int. Conf. Computer Design (ICCD)*, 2007, pp. 518–525.

[5] J. C. M. Li and E. J. McCluskey, "IDDQ data analysis using current signature," in *Proc. IEEE Int. Workshop IDDQ Testing*, 1998, pp. 37–42.

[6] L. E. Dermentzoglou, A. Arapoyanni, and Y. Tsiatouhas, "A built-in-test circuit for RF differential low noise amplifiers," *IEEE Trans. Circuits Syst. I*, vol. 57, no. 7, pp. 1549–1558, 2010.

[7] K. Suenaga, R. Picos, S. Bota, M. Roca, E. Isern, and E. Garcia-Moreno, "Parametrical fault test of CMOS LNA," in *Proc. 7th Int. Caribbean Conf. Devices, Circuits and Systems (ICCDCS)*, 2008, pp. 1–6.

[8] J. Liaperdos, A. Arapoyanni, and Y. Tsiatouhas, "A test and calibration strategy for adjustable RF circuits," *Analog Integrated Circuits and Signal Processing*, vol. 74, no. 1, pp. 175–192, 2013.

[9] J. P. Shen, W. Maly, and F. J. Ferguson, "Inductive fault analysis of MOS integrated circuits," *IEEE Des. Test. Comput.*, vol. 2, no. 6, pp. 13–26, 1985.

[10] T. Olbrich, J. Pérez, I. A. Grout, A. M. D. Richardson, and C. Ferrer, "Defect-oriented vs schematic-level based fault simulation for mixed-signal ICs," in *Proc. Int. Test Conf.*, 1996, pp. 511–520.

[11] Y. Xing, "Defect-oriented testing of mixed-signal ICs: Some industrial experience," in *Proc. IEEE Int. Test Conf.*, 1998, pp. 678–687.

[12] E. Acar and S. Ozev, "Defect-oriented testing of RF circuits," *IEEE Trans. Comput.-Aided Design Integr. Circuits Syst.*, vol. 27, no. 5, pp. 920–931, 2008.

[13] R. Kheriji, V. Danelon, J. L. Carbonero, and S. Mir, "Optimising test sets for RF components with a defect-oriented approach," in *Proc. ICM 16th Int. Conf. Microelectronics*, 2004, pp. 400–403.

[14] K. Arabi and B. Kaminska, "Design for testability of embedded integrated operational amplifiers," *IEEE J. Solid-State Circuits*, vol. 33, no. 4, pp. 573–581, 1998.

[15] H. G. Stratigopoulos, J. Tongbong, and S. Mir, "A general method to evaluate RF BIST techniques based on non-parametric density estimation," in *Proc. Design, Automation and Test in Europe, (DATE)*, 2008, pp. 68–73.

[16] K. Huang, H. G. Stratigopoulos, and S. Mir, "Bayesian fault diagnosis of RF circuits using nonparametric density estimation," in *Proc. 19th IEEE Asian Test Sym. (ATS)*, 2010, pp. 295–298.

[17] K. Huang, H. G. Stratigopoulos, S. Mir, C. Hora, Y. Xing, and B. Kruseman, "Diagnosis of local spot defects in analog circuits," *IEEE Trans. Instrum. Meas.*, vol. 61, no. 10, pp. 2701–2712, 2012.

[18] R. Rodriguez-Montanes, E. Bruis, and J. Figueras, "Bridging defects resistance measurements in a CMOS process," in *Proc. Int. Test Conf.*, 1992, pp. 892–899.

[19] J. H. Friedman, "Multivariate adaptive regression splines," *Ann. Stat.*, vol. 19, pp. 1–141, 1991.

[20] R. Rodriguez-Montanes, J. P. de Gyvez, and P. Volf, "Resistance characterization for weak open defects," *IEEE Des. Test. Comput.*, vol. 19, no. 5, pp. 18–26, 2002.